Journal of Materials Science Research and Reviews

6(1): 37-54, 2020; Article no.JMSRR.61050

Mechanical Characterization of Fe-Co-2V (Hiperco): Fatigue/Monotonic Testing, Hardness Testing and Fractography

Elisabeth Keller[1,2], Tariq A. Khraishi[1*] and Kyle Johnson[2]

[1]Mechanical Engineering Department, University of New Mexico, Albuquerque NM, USA.
[2]Sandia National Laboratories, Albuquerque NM, USA.

Authors' contributions

This work was carried out in collaboration among all authors. Author EK performed a lot of the sample testing and processing of data, as well as writing. Author TK assisted with sample testing and data selection/processing, as well as writing. Author KJ originally conceived the project idea, contributed to all discussions and planned procedures and contributed to the writing. All authors read and approved the final manuscript.

Article Information

Editor(s):
(1) Dr. Yong X. Gan, California State Polytechnic University, USA.
Reviewers:
(1) Pankaj Kumar, SR University, India.
(2) M. V. Praveen Kumar, India.
Complete Peer review History: http://www.sdiarticle4.com/review-history/61050

Original Research Article

Received 02 July 2020
Accepted 08 September 2020
Published 19 September 2020

ABSTRACT

Fe-Co-2V is a popular metallic alloy used in electromagnetic applications. However, there is a lack of mechanical fatigue characterization of this alloy in the literature. In this work, Fe-Co-2V specimens with rectangular cross-sections were carefully prepared in accordance with standards. They were measured for surface roughness and then subjected to quasi-static monotonic testing, as well as fatigue testing at both 0.5 Hz and 1 Hz frequencies. Both Rockwell hardness and Vickers micro-hardness testing were performed. Additionally, scanning electron microscopy imaging of the fractured surfaces was done. The quasi-static testing revealed a flat yield region characteristic of Lüders bands. The fatigue results did not show significant differences or sensitivity to change in frequency, although the fatigue life was higher on average for the 0.5 Hz. However, the fatigue results differed from published work at 0.33 Hz. The fractography revealed purely brittle fracture, with clear chevron marks and fracture initiation always starting at the surface. Lastly, it was identified that the C, D, and F Rockwell hardness scales were appropriate for testing this material and that the grain size necessitated the use of the upper end of indentation force for Vickers micro-hardness testing.

**Corresponding author: Email: khraishi@unm.edu;*

Keywords: Hiperco; fatigue; quasi-static; Lüders bands; Vickers; Rockwell; surface roughness.

1. INTRODUCTION

The metal alloy comprised of iron, cobalt, and vanadium (Fe-Co-2V) is commonly known as Hiperco®, a registered trademark of Carpenter Technologies. It typically has low ductility and soft metallic properties in accordance with Sundar and Deevi [1]. It is expensive (up to $239 per kilogram) due to the cobalt component. Hiperco also has the highest saturation induction of all metal alloys, high permeability, high Curie temperature, and low coercivity and core loss. The vanadium component increases its ductility as well as the electrical resistivity. Without vanadium, the Fe-Co is too brittle to be industrially produced [2]. Hiperco is used in electromagnetic applications such as solenoids, electric motors, and generators where weight or space is important [3]. Hiperco has high magnetic saturation which allows it to be used in aircraft generators [4].

In its ordered B2 state, Hiperco acts like other ordered structures and its grain boundaries are barriers to dislocations [5]. Pitt and Rawlings [4] experimented with tensile testing of Hiperco as well as Fe-Co-V-Ni to determine the microstructural features that impacted both the Lüders strain and ductility of these materials. Kustas et al. [6] experimented with additive manufacturing of Fe-Co-1.5V. The authors mentioned that typical Hiperco has low workability that can be improved using 3D printing. Ren et al. [7] experimented with Hiperco and Fe-27Co. They performed different strain-rate tensile testing on specimens that were heat-treated at various temperatures. A micro-hardness test was performed on a similar alloy, i.e. FeCo-2V with 0.04Nb [8]. Nabi et al. [8], showed that coercivity and strength as a function of heat treatments are related to grain boundary spacing and degree of order. For this current work, the Vickers micro-hardness test displays the impact of the grain size and boundaries on the resulting indentation shape. Studies show that most Fe-Co alloys' yield strength is primarily controlled by grain size [2]. Grain size for Hiperco was measured by Susan et al. [9] for 1-inch and 2-inch diameter bars heat-treated at 838°C for two hours. The grain sizes towards the center of the bar are smaller than the grain sizes towards the outside edges due to different times at temperature. The grain size range relevant to the current work is from the 1-inch diameter bar; about 35 to 40 microns.

Fatigue is the weakening of material caused by repeatedly, or cyclically, applied loads [10]. Thus, fatigue failure is the failure of the material after a load has been repeatedly applied. Fatigue failure often gives no warning and the specimens will quickly break [10]. This applied dynamic loading and unloading can cause the material to fail at lower loads than under a static load. Static loads fail because the stress has exceeded the yield strength whereas fatigue failure can occur below the yield strength [10].

The fatigue process consists of the following steps (Budynas and Nisbett 2015) [10]:

- Stage I Initiation of one or more microcracks due to cyclic plastic deformation
- Stage II The microcracks progress into macrocracks
- Stage III The remaining material cannot support the loads, resulting in fracture

Table 1. Similarities and differences between experimental approach of this paper and Stoloff et al. [11]

Testing Condition	Stoloff et al.	This Work
Heat Treatment	1000 °C	838 °C
Specimen Geometry	Dog-Bone, Cylindrical Cross-Section	Dog-Bone, Rectangular Cross-Section
Frequency Tested	0.33 Hz	0.5 and 1 Hz
Microstate	Ordered and Disordered	Ordered
Fatigue Control Type	Strain-Controlled	Strain-Controlled
Fatigue Testing Type	Fully Reversed Tension-Compression	Fully Reversed Tension-Compression
Testing Environment	Air and Vacuum	Air

There are three major methods used to study fatigue life in design and analysis [10]. They include stress-life, strain-life, and linear elastic fracture mechanics. This research conducted fatigue testing with controlled cyclic strain.

Hiperco has undergone fatigue testing in the past. Stoloff et al. [11] tested ordered and disordered Hiperco in air and in vacuum. This current paper's conditions vs Stoloff et al.'s are displayed in the Table 1.

2. MATERIALS AND METHODS

2.1 Specimen Preparation

The Hiperco specimen geometry used in this study is shown in Fig. 1. The figure shows suggested ranges for the different dimensions as in the ASTM standard E606/E606M-12 [12] for fatigue testing for a flat-sheet specimen with a rectangular cross section. All specimens were cut out of two 1-meter long bars of Hiperco with 1-inch diameter each. To optimize the total number of specimens obtained from the bars, the following dimensions were chosen: Thickness (T) = 0.157 in (3.99 mm), Width (W) = 0.63 in (16 mm), Length (L) = 0.6 in (15.24 mm), Grip Length (G) = 1.24 in (31.5 mm), Fillet Radius (R) = 0.63 in (16 mm).

When comparing the actual dimensions used here to the standards, it is shown that the width is within the range for all specimens. The length of the specimens is longer than that of the standards by less than 10%. This provided enough room for the extensometer to be placed directly in the middle of the specimen. The grip length is smaller than the standard; whereas the fillet radius is almost double that of the standard (towards the higher part of the range). An increased fillet radius is generally a good thing as it allows smoother transition of force lines from the grip area to the gauge area. Fig. 2 shows some of the specimens cut out from a bar as they were still in preparation.

To prepare the specimens, the wrought Hiperco bar was cut into two halves using a water-jet axially along a symmetry plane. Each of the halves was cut into dog-bone shapes using a CNC machine (Haas Automation, Inc. Model VF-2, serial number 1131690). Each specimen was then semi-polished using an automated precision grinder (Harig, 618 Automatic) and later on lightly by hand using fine grit sandpaper. The specimens were then heat treated at a temperature of 838 ^{o}C in a vacuum furnace for a dwell time of two hours and then after furnace cooling were immediately placed in air-sealed plastic bags for experimentation.

2.2 Quasi-Static Testing

The quasi-static tests were performed on an MTS 500 kN (110 kip) load frame (Model 312.41), an MTS 250 kN (55 kip) load cell (Model 661.23A-01), and MTS 647 Hydraulic wedge grips. These wedge grips were fatigue-rated with dynamic force capacity of 100 kN (22 kip) as well as having a static force capacity of 120kN (27 kip). The displacement rate for the tension tests was 0.015 mm/s.

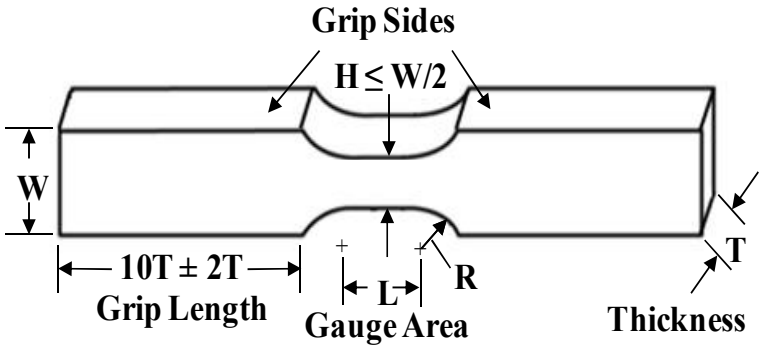

Fig. 1. ASTM Standard E606/606M-12 [12] for a flat-sheet specimen with a rectangular cross section

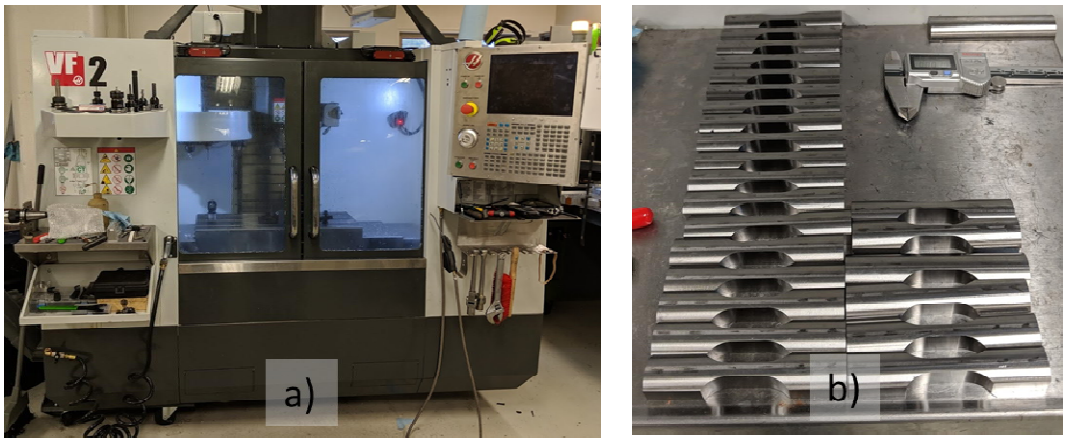

Fig. 2. (a) The CNC machine, (b) Specimens after being cut

2.3 Fatigue Testing

The fatigue tests were performed on the same MTS machine as quasi-static testing. The specimen setup is displayed in Fig. 3. The controller for the MTS machine was MTS FlexTest 40, Digital Controller, Model 494.04, and the software used was MTS Flex Test (TM) 40, Station Manager, Version 5.9E 6058.

The specimens were handled with gloves during the process of marking each specimen name and the gauge length boundaries. The extensometer used in the testing was an MTS 0.5-inch gauge extensometer (Model 634.31E-24). Gloves were also worn during the process of positioning the extensometer onto the specimen to limit any possible contamination. The extensometer was placed in the middle of the gauge area and held in place with rubber bands.

The fatigue loading applied for every test was a fully-reversed sinusoidal waveform under strain control. The strain amplitudes for the 1 Hz testing were 0.15%, 0.20%, 0.25%, 0.30%, 0.40%, and 1%. The strain amplitudes for the 0.5 Hz testing were 0.15%, 0.20%, 0.25%, and 0.30%.

The Coffin-Manson equation is a relationship between fatigue life and the applied strain amplitude (Budynas and Nisbett 2015) [10]. The equation is as follows:

$$\frac{\Delta\varepsilon}{2} = \frac{\sigma_f^{'}}{E}(2N_f)^b + \varepsilon_f^{'}(2N_f)^c \quad (1)$$

Where $\frac{\Delta\varepsilon}{2}$ is the total strain amplitude, $\sigma_f^{'}$ is the fatigue coefficient, E is Young's modulus, $2N_f$ is the number of reversals to failure (which is twice the number of cycles to failure), b is the fatigue strength exponent, $\varepsilon_f^{'}$ is the fatigue ductility coefficient, and c is the fatigue ductility exponent.

The first part of Equation 1, $\frac{\sigma_f^{'}}{E}(2N_f)^b$, is the elastic portion of the total strain amplitude. The second part of Equation 1, $\varepsilon_f^{'}(2N_f)^c$, is the plastic portion of the total strain amplitude. The equation can be re-written in the following way:

$$\frac{\Delta\varepsilon}{2} = a(2N_f)^b + d(2N_f)^c \quad (2)$$

Where a is $\frac{\sigma_f^{'}}{E}$, b is the same, c is the same and d is $\varepsilon_f^{'}$. These four unknowns in Equation 2 can be found using an error minimization process. This process uses an initial guess for three of the four variables/parameters and varies the fourth variable until the error is minimized. Then that variable is fixed at the found value and the next variable is varied holding the others constant. The initial guesses/ranges for the parameters were based on the work of Johnson et al. (2016) [13] who experimented with wrought Inconel 718 to fit a Coffin-Manson curve. This process continues until all four variables/parameters have been optimized. In terms of computer coding, this is the equivalent of four nested loops needed for such error minimization. The error formula is given below (see Equation 4) although it can be normalized by n (the total number of specimens).

The correlation coefficient between the data points and the curve is known as R^2, also known as a "goodness of fit" parameter. The following formulas (Chapra and Canale 2002) [14] are used to calculate R^2:

$$S_t = \sum(y_i - \overline{y})^2 \quad (3)$$

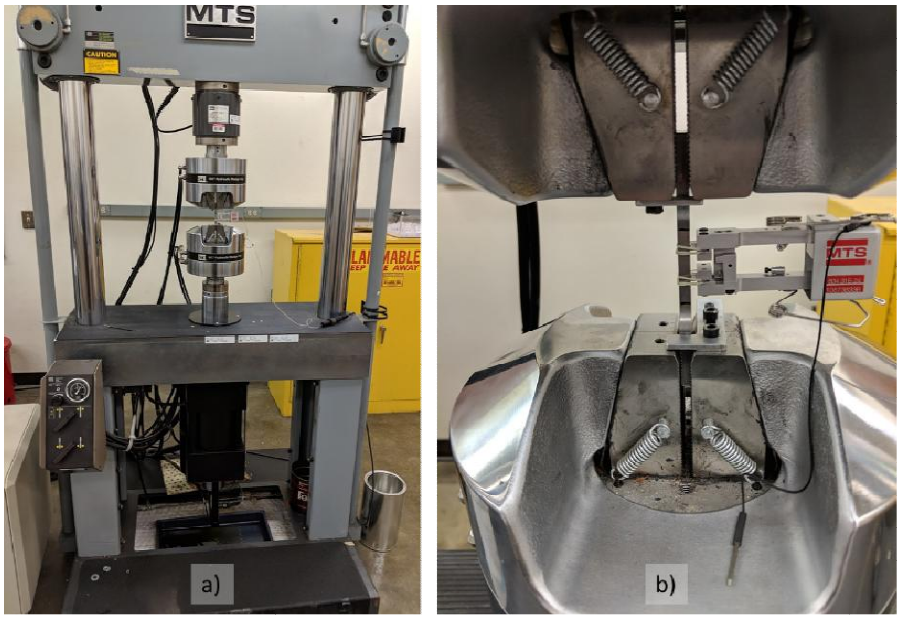

Fig. 3. (a) The MTS machine with the specimen, (b) A close-up on the gripped specimen with the extensometer attached

In Equation 3, S_t is the total sum of the squares of the residuals between the data points and the mean $\overline{y}$.

$$S_r = \sum\left(y_{i,measured} - y_{i,model}\right)^2 \quad (4)$$

In Equation 4, S_r is the sum of the squares of the residuals between the measured y and the calculated (i.e. model predicted) y values. The summation is over the range of the experimental data points. Equation 5 uses both S_t and S_r from equations 3 and 4, respectively, to find R^2.

$$R^2 = \frac{S_t - S_r}{S_t} \quad (5)$$

The closer the correlation coefficient is to 1, the more correlated the data is with the curve, i.e. the less the error in describing the data points with the chosen curve-fit equation.

2.4 Surface Roughness Measurements

The Mitutoyo surface roughness tester (Mitutoyo, SJ-210) was calibrated using a precision reference sample supplied by the manufacturer. The specimens were measured for roughness along the grip length sides. Due to the specimen preparation procedure, those potentially had the most surface roughness. The surface roughness tester works through reciprocating strokes and generates a surface profile for roughness from which the Ra metric, or other metrics, can be calculated. The goal for this roughness measurement was to ensure that specimens are under 12 micro-inches in roughness so as fatigue life is not impacted by large variations in surface roughness.

2.5 Hardness Tests

Indentation tests to measure hardness were performed using a Rockwell hardness tester (Buehler Rockwell/Superficial Type, Macromet II, Hardness Tester, Model number: 1800-2000) and a Vickers micro-hardness tester (Buehler Micromet, serial number BM83104). Rockwell hardness has different scales for testing. These scales differ in the amount of applied loading, as well as the type of indenter tip used (Khraishi and Al-Haik 2011) [15]. With respect to the Rockwell tester, several test scales were utilized in order to find which ones are appropriate for Hiperco. The F scale (60 kgf, indentation tip = 1/16 inch diameter (1.588 mm) steel sphere), C scale (150 kgf, indentation tip = 120° diamond sphero-conical), and D scale (100 kgf, indentation tip = 120° diamond sphero-conical) turned out to be appropriate for this material. Rockwell C is commonly used for materials such as steel, and scale D is used for thin steel. Rockwell F is commonly used for annealed copper alloys and thin soft sheet metals (Khraishi and Al-Haik 2011) [15]. The load was applied for 10 seconds

and the indentations spots were separated by about five indentation diameters.

Vickers micro-hardness testing uses a four-faceted diamond indenter tip that leaves ideally an imprint of a diamond shape with two diagonals. Then the diagonal lengths are measured, and the mean of both diagonals is used in the hardness calculation. The applied force used in this work was 1 kg. The Vickers micro-hardness (HV) is given by the following equation:

$$HV = \frac{Test\ load\ (kgf)}{Surface\ area\ of\ indentation\ (mm^2)} = 1854 * \frac{1}{\left(\frac{d_1 - d_2}{2}\right)^2} \quad (6)$$

For the Vickers test, standard test blocks were first used to ensure the machine and attached computer software were calibrated. Then load was applied for fifteen seconds for each indentation/hardness test. The ensuing diamond diagonal length was measured first using the eyepiece and then confirmed via digital imaging and metallurgical computer software (Buehler OmniMet for Matrox Mil 10, 10.0.6.0).

As mentioned prior, the specimens were semi-polished using a precision grinder. Under a microscope, the semi-polished surface exhibits ridges or lines. In order to remove the ridges, one of the untested semi-polished specimens was polished by cutting a piece out and then placing it in a fast-drying epoxy resin in a rubber mold. The piece was then polished on polishing wheels using diamond particle pastes of 1 micron and then 0.25 microns. The specimen piece was cleaned using distilled water and dried using compressed air. The polished specimen, which had no visible ridges under the microscope, allowed for comparison with the Vickers results from the semi-polished specimens since it was anticipated that the surface roughness might have an impact on the measured diamond diagonal, and therefore on the calculated hardness.

3. RESULTS AND DISCUSSION

3.1 Quasi-Static Testing

Six of the Hiperco specimens underwent quasi-static testing. Two of the specimens had not undergone heat-treatment, while the other four specimens were heat-treated. Fig. 4 shows the tensile test results.

In the stress-strain curves, one can identify a flat yield region (also called “yield point elongation” in the literature) following the linear regime/high yield point. Such regions of perfectly-plastic flow are characteristic of low-carbon steels and indicative of Lüders bands formation. The average yield stress in the region is 275.79 MPa (40 ksi) for the heat-treated specimens. Wrought steels have a yield stress of 204.8 MPa to 1.723 GPa (29.7 ksi to 250 ksi) and an elastic modulus of 190.3 GPa to 210.3 GPa (27.6 msi to 30.5 msi) (Kalpakjian and Schmid 2014) [16]. Cobalt’s elastic modulus is 211.0 GPa (30.6 msi) and yield stress is 344.7 MPa (50 ksi) (Kobayashi and Suzuki 2013) [17]. Hiperco’s elastic modulus was found to be 230.3 GPa (33.4 msi) which is a little outside the range for wrought steel indicating the effect of cobalt (which is half of the composition). This elastic modulus value is consistent with previously reported values [18]. Steel’s elastic modulus does not change much due to heat treatment or typical alloying (Kalpakjian and Schmid 2014) [16].

Fig. 4 shows a clear drop in yield stress and the increase in strain-to-failure with heat treatment. The ultimate tensile strength also increases with heat treatment. This is not common for typical heat-treated metal. Usually, lower yield stress would also equate to a lower ultimate tensile stress. For Hiperco, this is not the case due to the increased strain-to-failure and little effect of heat treatment on hardening modulus. The drop in the yield stress with heat treatment has also been reported by Ren et al. (2001) [7].

Specimens 24 and 25 in Fig. 4 were not pulled to failure/rupture. The average strain percentage that the heat-treated specimens fractured at was 7%. The average strain percentage that the specimens started yielding at was 0.12%. The specimens that were later fatigue tested were mainly in the plastic regime of Fig. 4 in terms of the quasi-static yield stress values; the specimens tested at 0.10% strain amplitude were in the elastic range.

3.2 Fatigue Testing

The first set of Hiperco fatigue specimens were tested at 1 Hz. Fig. 5 displays the specimens tested at the strain amplitudes displayed in the legend. There were two specimens tested at 0.30%, 0.25%, 0.20%, 0.15%, and 0.10%. The results of these specimens that were tested at the same strain amplitude are all close to each other. The two specimens tested at 0.10% strain

amplitude were not tested to failure (and hence the arrow on them pointing to the right). They were stopped within 11.6% of each other. Because these specimens did not fail, they were not included in the data used for curve fitting the Coffin-Manson relationship. Each specimen that was tested at the same strain amplitude had a similar number of cycles to failure. Also, the force level at the 1% strain did not stabilize like the other specimens, although it broke off cleanly within the gauge area and showed progress towards stabilization.

The second set of Hiperco specimens were tested at 0.5 Hz. Fig. 6 displays those specimens at the strain amplitudes displayed in the legend. Here, four specimens were tested for each of the strain amplitudes. Each strain amplitude at 0.5 Hz has a wider range for the number of cycles and the testing therefore was not as consistent as for the 1 Hz. However, only 2 specimens per strain amplitude were tested for the 1 Hz whereas 4 specimens were tested for the 0.5 Hz. Having been able to test more specimens per strain amplitude for the 1 Hz could have produced a wider range of results. The temperature for all tests varied by about 3°C.

The hypothesis by the authors before conducting the 0.5 Hz testing was that the cycles to failure at

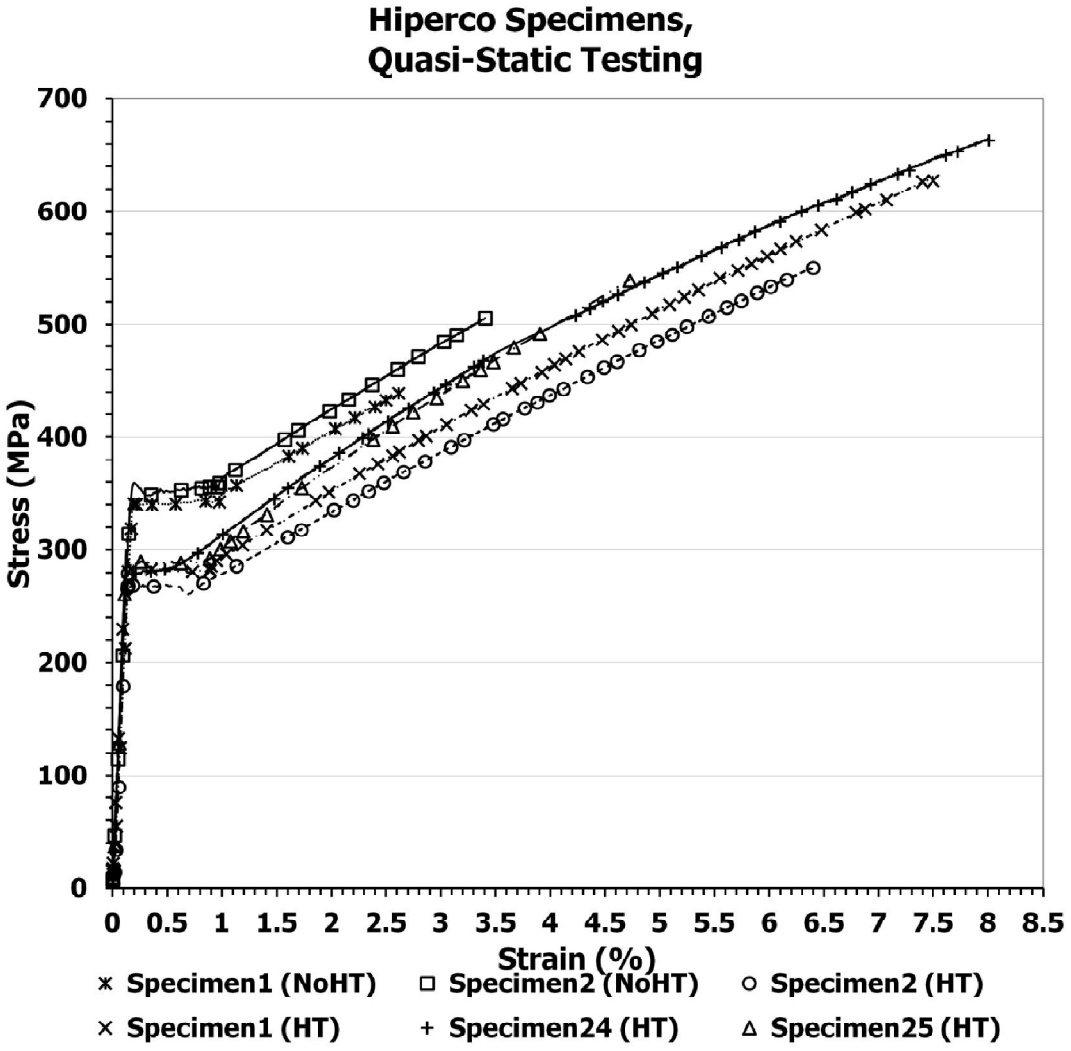

Fig. 4. Quasi-static testing results, stress vs strain
HT = Heat-treated, NoHT = Not heat-treated

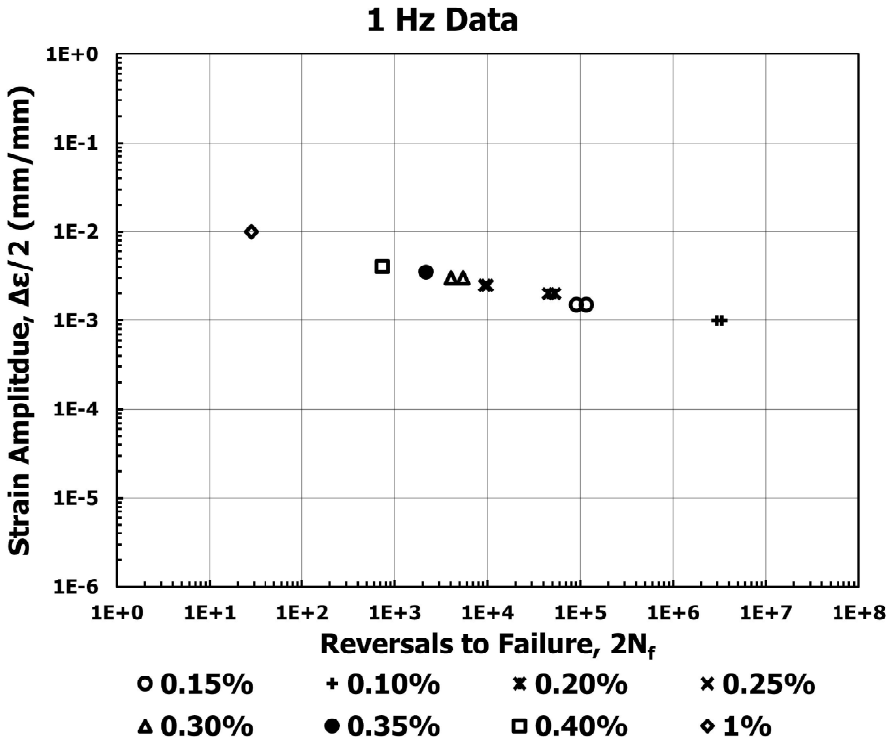

Fig. 5. Plot of fatigue testing results at 1 Hz

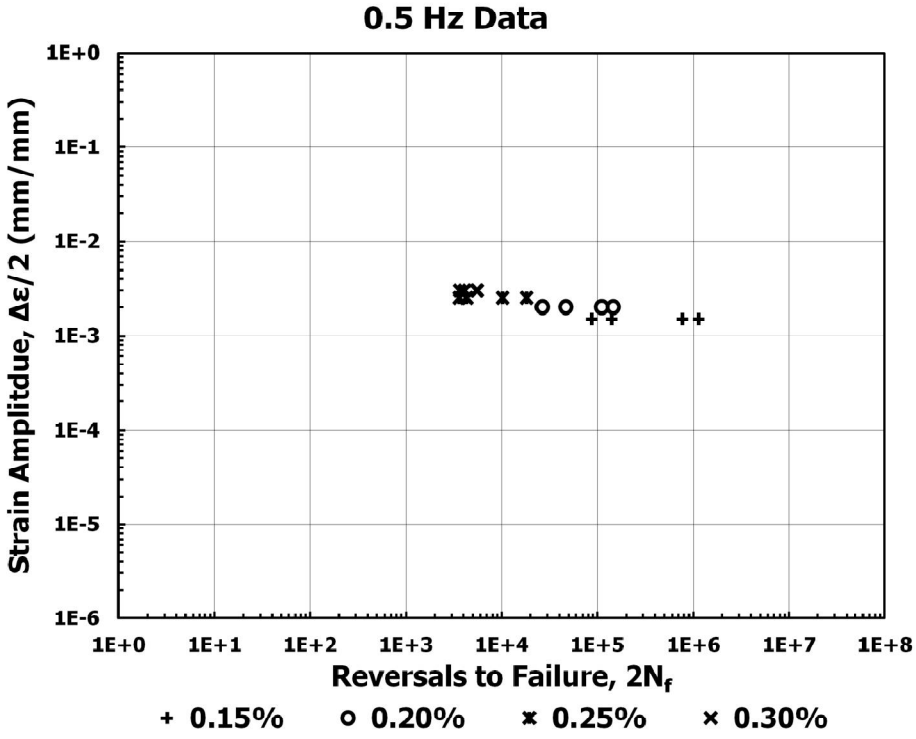

Fig. 6. Plot of fatigue testing results at 0.5 Hz

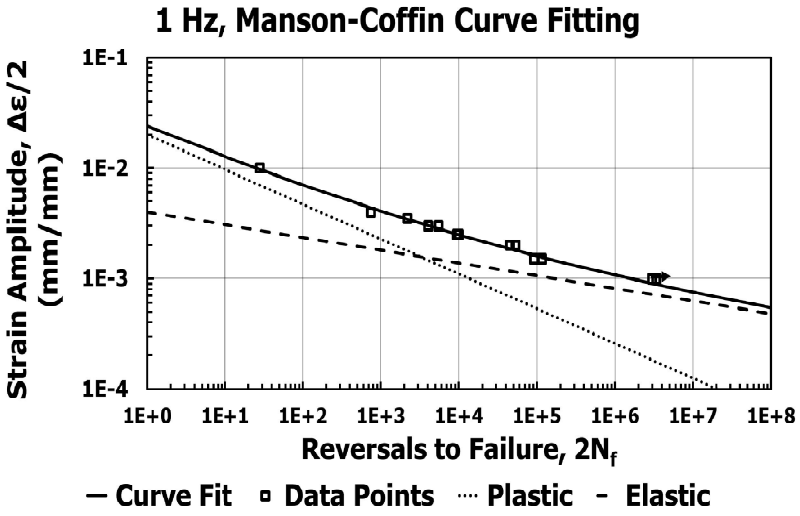

Fig. 7. Coffin-Manson curve fitting for 1 Hz fatigue results

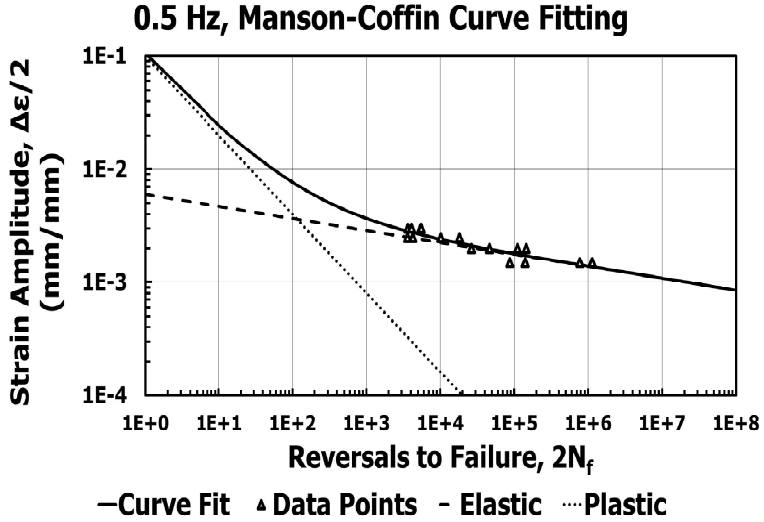

Fig. 8. Coffin-Manson curve fitting for 0.5 Hz fatigue results

this slower frequency would be higher than for the 1 Hz. This is because of the underlying physics. At a higher frequency, there is more heat produced in a given time period, allowing more dislocation motion activation, resulting in a shorter number of cycles to failure. At the slower frequency there is less heat produced, therefore the dislocations move more slowly. From the testing results and on average, the 0.5 Hz specimens needed more cycles to failure than the specimens at 1 Hz.

The Coffin-Manson curve fitting, Equation 1, was applied to these fatigue plots using the optimization scheme described above. The fitted parameters for the fatigue testing at 1 Hz are $\frac{\sigma_f^{'}}{E}$ = 0.004, b = -0.115, $\varepsilon_f^{'}$ = 0.02 mm/mm, and c = -0.315. The fitted parameters for the fatigue testing at 0.5 Hz are $\frac{\sigma_f^{'}}{E}$ = 0.006, b = -0.106, $\varepsilon_f^{'}$ = 0.099 mm/mm, and c = -0.697. Figs. 7 and 8 show the curve fitting along with the experimental data points it was derived from.

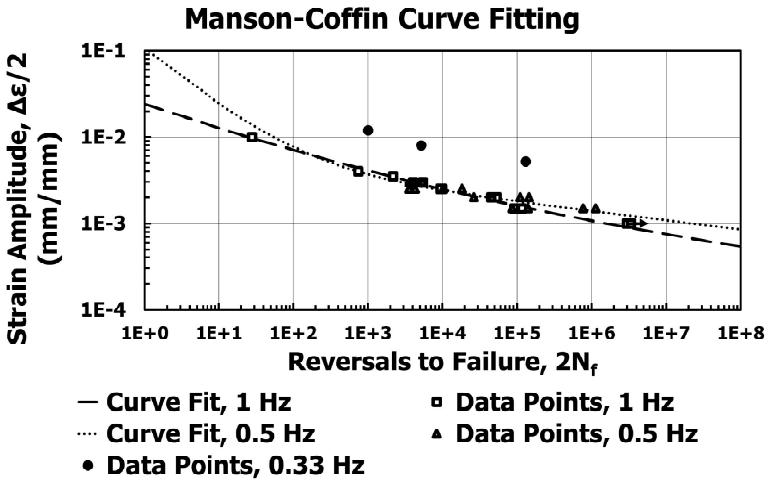

Fig. 9. Fatigue testing for 1 Hz and 0.5 Hz along with experimental data. Also included is the data by Stoloff et al. [11]

Fig. 9 displays the data for the 1 and 0.5 Hz conducted in this research as well as the 0.33 Hz from the testing conducted by Stoloff et al. [11] for ordered specimens (i.e. heat-treated). The combined data in this figure indicate that the data from the two frequencies are essentially overlapping, with the 0.5 Hz showing more shift to the right with lower strain amplitudes as was predicted to happen. The calculated R^2 for 0.5 Hz is 0.98 and for 1 Hz is 0.99. The curve for 1 Hz is flatter than for 0.5 Hz which shows more curvature. This could be due to the aforementioned statement about the 1% data point not reaching force stabilization.

The fact that the data points from the two frequencies are not much different, i.e. mostly overlapping, is not really surprising for two reasons. First, the two frequencies are not very different in magnitude, e.g. they are not order(s) of magnitude different. Second, the mode of failure is brittle (more on this later) and hence there is a limited role for plasticity and dislocations in determining fatigue life.

Notice that the 0.33 Hz data by Stoloff et al. [11] is significantly different than the current data. There are two potential reasons for that. First, their data was based on a different heat treatment (1000 ^{o}C versus 838 ^{o}C). Second, their samples were cylindrical and here the samples were rectangular in cross-section. Cylindrical samples in general have longer fatigue life compared to rectangular (Lewis and Janna, 2003) [19].

3.3 Hardening Behavior with Cycling

An important thing to consider for strain-controlled fatigue testing is whether or not hardening, i.e. increased sustained stresses beyond yield stress, occurs over time. For strain-controlled tests this effect is often shown by S-N curves, i.e. plots of stress amplitude versus the number of cycles. This is done here in Figs. 10-13 for 0.5 Hz. In Fig. 10, the specimens tested at 0.30% strain all demonstrated similar hardening behavior. The range of stress at fracture is from 550 to 700 MPa, a difference of 150 MPa. In Fig. 11, the specimens tested at 0.25% strain all demonstrated similar hardening behavior like the specimens tested at 0.30% strain. The range of stress at fracture is from 450 to 600 MPa, a difference of 150 MPa. As expected, there is less overall hardening than the 0.3% samples. In Fig. 12, the S-N curves for 0.20% strain amplitude are shown. The range of the stress at fracture is from 410-560, with a difference of 150 MPa. In Fig. 13, the range of the stress at fracture for the 0.15% samples is from 320-430, with a difference of 110 MPa.

There are a few insights extracted from these figures. First, they all demonstrate clearly the hardening behavior that is taking place during fatigue testing. Second, with higher strain amplitude, the hardening amount should go up, and that is mostly reflected in these figures. Third, the curves show the force stabilization over time that these specimens experienced; an important distinction for defining a good sample with good data for inclusion here. Fourth, all the

curves seem to have an initial linear growth in their profile followed by non-linear behavior leading to a plateau, i.e. force stabilization. Fifth, the maximum stress encountered by the samples was commensurate with the range of ultimate stresses seen in the quasi-static testing (Fig. 4).

3.4 Surface Roughness Testing

Using the Mitutoyo surface tester, the surface roughness of the grip sides was measured for 30 samples. The results of the testing are shown in Table 2.

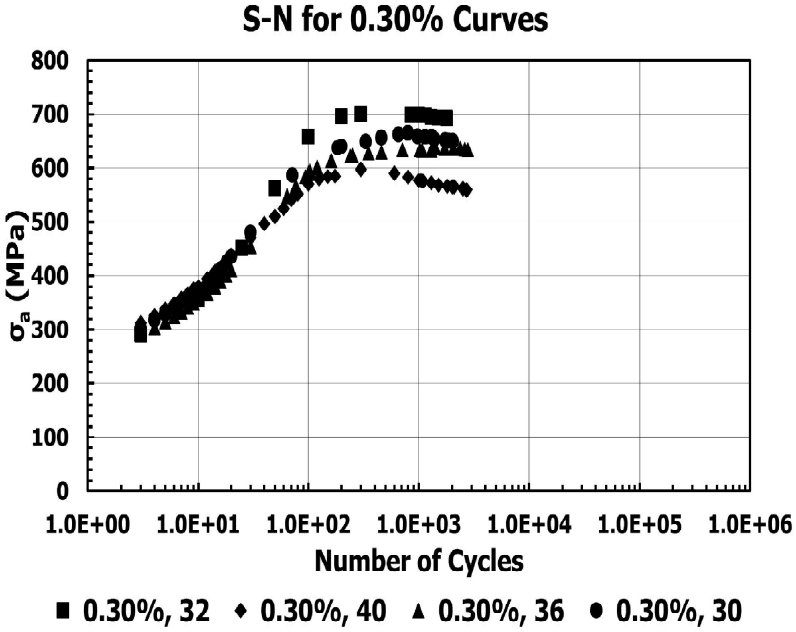

Fig. 10. S-N curve at 0.5 Hz for 0.30% strain amplitude.
The numbers 30, 32, 36 and 40 are sample numbers

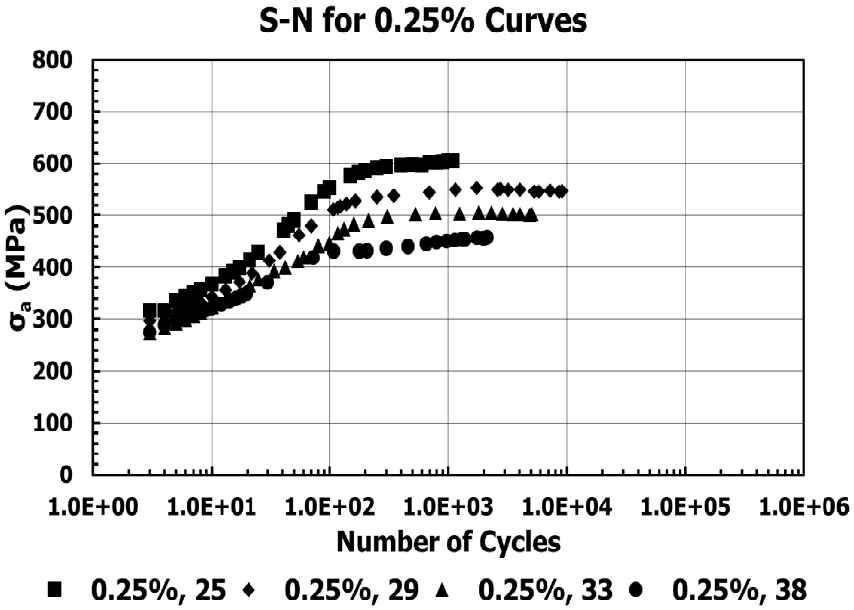

Fig. 11. S-N curve at 0.5 Hz for 0.25% strain amplitude
The numbers 25, 29, 33 and 38 are sample numbers

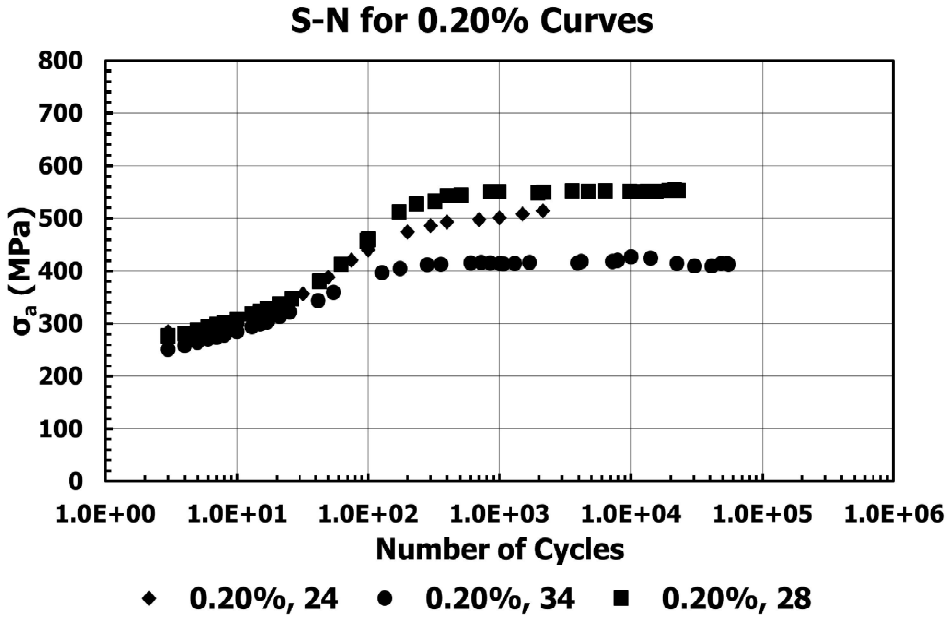

Fig. 12. S-N curve at 0.5 Hz for 0.20% strain amplitude
The numbers 24, 28 and 34 are sample numbers

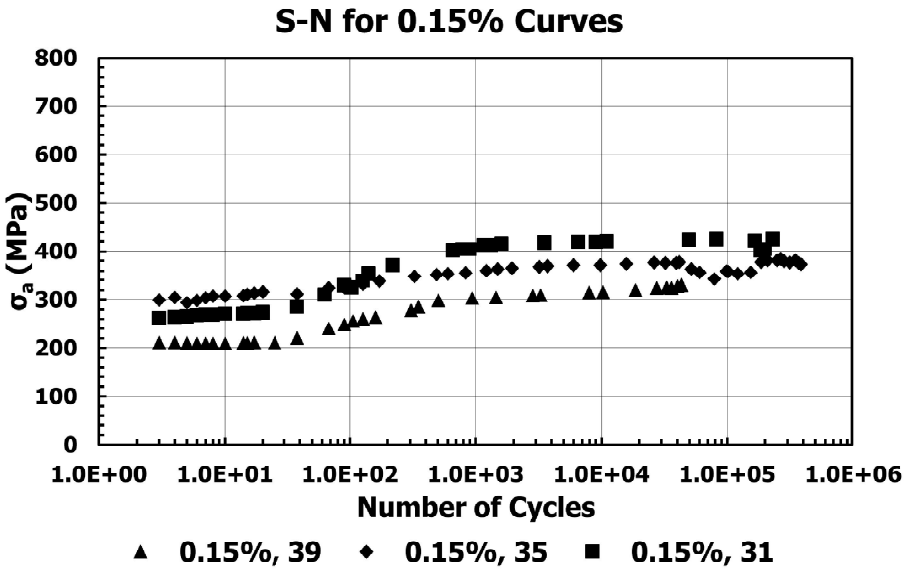

Fig. 13. S-N curve at 0.5 Hz for 0.15% strain amplitude
The numbers 31, 35 and 39 are sample numbers

Table 2. Surface roughness average and standard deviation for 30 Hiperco samples. Each sample underwent 10-15 roughness readings. Here Ra was measured (i.e. the arithmetic average of the roughness profile)

Surface Roughness:	Number
Overall Average (μm):	0.2876
Overall Standard Deviation (μm):	0.0510
Readings Range (μm):	0.1777-0.5648

Table 3. Hiperco Rockwell hardness tests for C, D, and F scales

Rockwell Hardness Scale	C (HRC)	D (HRD)	F (HRF)
Average Hardness	13.1547	35.380	7.4608
Standard Deviation	0.6880	0.5765	0.6452

Table 4. Vickers micro-hardness testing results

Specimens	Vickers Hardness Average (HV)	Vickers Hardness Std Dev (HV)
Semi-Polished Specimen	213.44	11.479
Polished Specimen	204.24	9.316

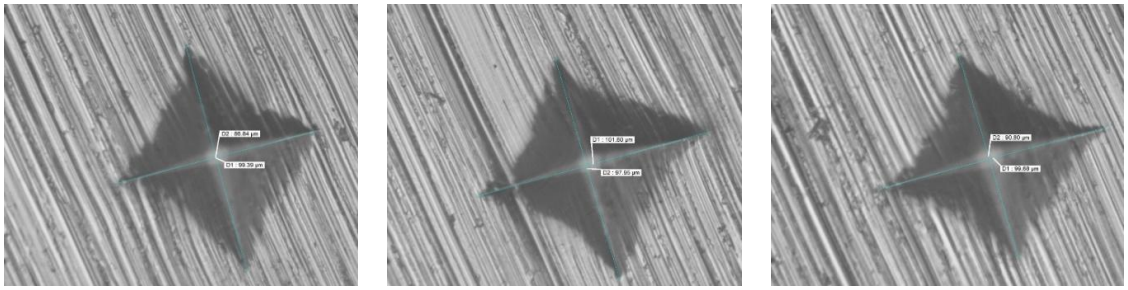

Fig. 14. Semi-polished specimen Vickers micro-hardness test indentations

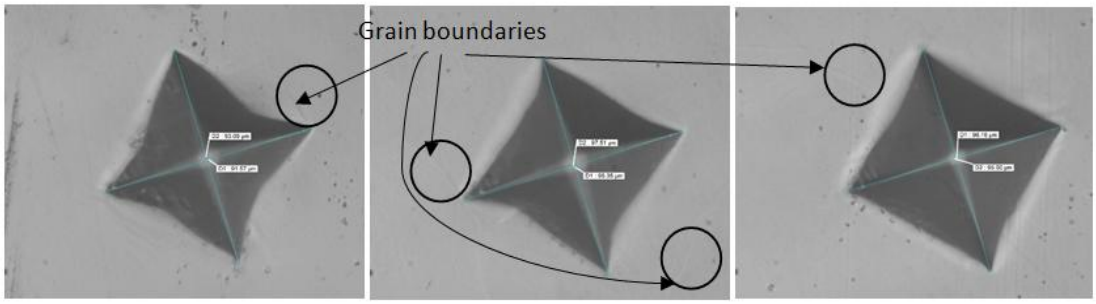

Fig. 15. Polished specimen Vickers micro-hardness test indentations

The main reason for performing the surface roughness measurements was to ensure that the machining specification of under 12 micro-inches (i.e. 0.3048 micrometers) was achieved, as it is known that surface roughness can impact fatigue life, i.e. the higher the surface roughness the lower the fatigue life (Kalpakjian and Schmid 2014) [16]. Therefore, the authors wanted to ensure that any variability in fatigue life was not due to large variability in surface roughness. Based on the roughness measurements, the possibility of such playing a major role in fatigue life is excluded, and the initial machining goal set prior to testing was achieved. More on the roughness below when micro-hardness testing is discussed.

3.5 Rockwell Hardness Testing

Hardness testing via indentations took place using a Rockwell tester. The hardness testing is another way of looking for consistency in the material and if lack of such consistency affected the fatigue results, i.e. caused any significant variations in fatigue life. Another reason for the testing was to identify which scales on the Rockwell tester (ASTM E 18-07 Standard Test Methods for Rockwell Hardness of Metallic Materials) were applicable or appropriate for the Hiperco material. After experimenting with the different scales, it was found that the C, D and F scales were appropriate. For the C-scale, 38 indentations were performed for data collection,

for the D-scale, 42 indentations were performed, and for the F-scale, 38 indentations were performed. Indentation locations were spaced at least five diameters apart. All surfaces indented here were semi-polished (see Table 2 for surface roughness). The testing results are shown in Table 3.

The Rockwell hardness of easily-machined steels is about 20 HRC [20]. Also, the Rockwell C hardness for annealed 416 stainless steel is 40 (https://www.beststainless.com/416-stainless-steel.html) and for annealed 316L stainless steel is 35. These annealed Hiperco results, from Table 3, are softer than all of the above.

3.6 Vickers Hardness Testing

Vickers micro-hardness testing (ASTM E92−17 Standard Test Methods for Vickers Hardness and Knoop Hardness of Metallic Materials) was performed on the semi-polished specimens as well as on polished specimens. The reason for polishing is that the Vickers testing is more sensitive to the surface condition or roughness compared to macro-scale indentation, e.g. Rockwell or Brinell. Here, the authors wanted to guard against the existence of surface roughness via the semi-polishing procedure, and ascertain any effect it may have had on the measured Vickers hardness values. For the semi-polished surface 49 indentations were performed, and for the polished surface 25 indentations were performed. Table 4 shows the Vickers hardness results.

The results of the Vickers micro-hardness tests are similar between the polished and semi-polished specimens, with a maximum difference of 4.5%. As a comparison, for different types of annealed stainless steel, the range of Vickers hardness is 200-240 [21]. Hiperco is within this range. The consistency of the Vickers results here adds further evidence that material inconsistency is not a factor in varied fatigue life at a given strain amplitude.

Figs. 14 and 15 show images of the indentation spots using the Vickers diamond tip. Fig. 14 shows 3 different indentations on the semi-polished surface exhibiting clear lines or ridges emanating from the precision or fine grinding. Fig. 15 shows 3 different indentations on a polished surface in which the ridges/lines were removed and a mirror-image surface was tested. On the polished specimen, the beginning and end of the diagonals are more clearly defined than the diagonals of the semi-polished specimens.

These figures show how both the semi-polished and the polished specimens have similar curvature or dips in the side edges of the indentation. The skewing of the indentation sides is likely an effect of the grain size being about half the indentation size, allowing for this non-uniformity. Indeed, in the polished images, one can observe grain boundaries around the indent. In addition, the ridges in the semi-polished specimen made it difficult to determine the exact of diagonal measurements. These ridges resulted in smaller diagonal sizes on average. When the indentation size is smaller, the hardness is higher (Equation 6).

3.7 Fractography

SEM images of the fracture surface were taken. The goal was to study whether the fracture whether is brittle, ductile, or in between. Fig. 16 shows an image of the overall fracture surface. Fig. 17 shows a close-up image of one of the corners of the fracture surface. For Fig. 16, several SEM images had to be pieced together to make this overall image due to the limited aperture involved. A darker contrast composition for the whole fracture surface was also taken but not shown here for brevity. The strain-amplitude utilized for this specimen was 0.15%.

It could be seen in Fig. 16 that there are Chevron marks leading to the top left corner of the fractured surface. Additional close-up images like Fig. 17 more clearly show the same. In such close-up images, it was clear that the initial fracture site/location was on the edges (i.e. on the external surface of the gauge section) and close to a corner of the rectangular fracture surface. Examining other specimens' fracture surfaces also revealed similar conclusions. Moreover, no striations or beach marks were captured in the images. Such striations would be indicative of a more ductile fracture that was progressive in nature. The reason the 0.15% strain sample was used here was because such specimens had longer life than other specimens with higher imposed strain amplitude. In other words, if there are striations to capture, they would be more easily captured with the low-strain samples than the high-strain samples. Another thing to point out in Fig. 17 is that there is a noticeable crack (shown in a circle) in the top left corner which appears perpendicular to the fracture surface. Upon examining several

Fig. 16. SEM of the whole fracture surface (lighter contrast)

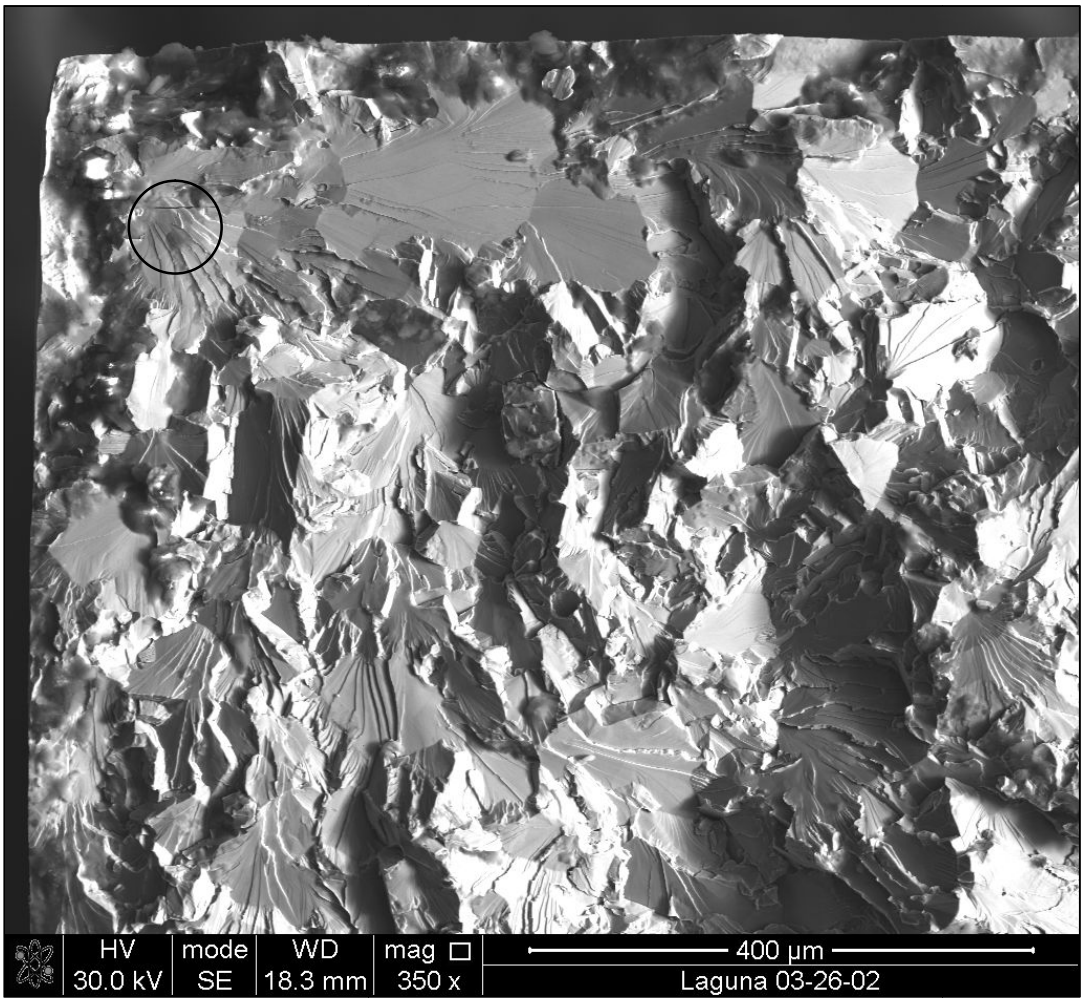

Fig. 17. Initial fracture corner/site on the surface

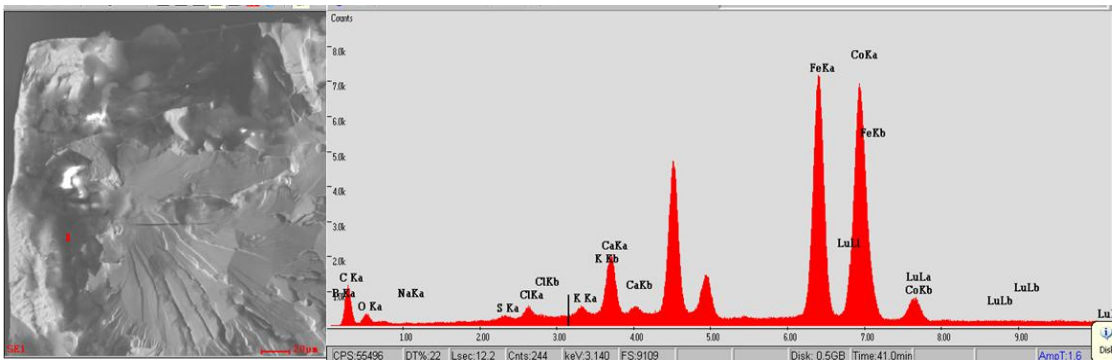

Fig. 18. Elemental analysis on a spot in the initial fracture site

Hiperco specimens, it was clear that fracture was of brittle nature and that this realization is commensurate with the relatively low fracture strain values encountered in quasi-static testing (Fig. 4).

3.8 Elemental Analysis

The SEM used had the capability of performing elemental analysis focused on any part of the

examined surface. This was performed at different spots on the surface with the goal of ensuring that the composition is dominated by iron and cobalt. Fig. 18 shows one such elemental scan that ensures so. The figure shows that iron and cobalt are the predominant elements in the alloy.

4. CONCLUSION

First, heat-treated Hiperco resulted in elongated strain-to-failure and lower yield stress but higher ultimate strength. The yield region was flat and characteristic of Lüders bands formation, similar to low-carbon steels. Second, the Coffin-Manson equation was used for fitting data points from fatigue testing of Hiperco at constant applied strain amplitude resulting in R^2 equal to at least 0.98. The fatigue results showed little sensitivity, and mostly in conjunction with lower applied strains, to changes in fatigue loading frequency from 0.5 Hz to 1.0 Hz. This work adds to the literature fatigue data at a different heat treatment and different frequencies than previously exists. Third, fatigue fracture was brittle in nature per fractography showing clearly formed chevron marks. Fourth, Rockwell scale C, D and F were found appropriate for hardness testing of Hiperco. Fifth, care should be taken when performing Vickers micro-hardness testing due to the underlying grains being similar in size to the indents. Therefore, the highest loads on the Vickers tester should be employed (1 kg force and higher recommended). The Vickers micro-hardness for Hiperco is similar to stainless steels.

ACKNOWLEDGEMENTS

This paper describes objective technical results and analysis. Any subjective views or opinions that might be expressed in the paper do not necessarily represent the views of the U.S. Department of Energy or the United States Government.

Sandia National Laboratories is a multi-mission laboratory managed and operated by National Technology and Engineering Solution of Sandia, LLC., a wholly owned subsidiary of Honeywell International, Inc., for the U.S. Department of Energy's National Nuclear Security Administration under contract DE-NA0003525.

COMPETING INTERESTS

Authors have declared that no competing interests exist.

REFERENCES

1. RS Sundar, SC Deevi. Soft magnetic FeCo alloys: alloy development, processing, and properties, International Materials Reviews, 50:3, 157-192, DOI:10.1179/174328005X14339
2. Sourmail T. Near equiatomic FeCo alloys: Constitution, mechanical and magnetic properties. Progress in Materials Science. 2005;50(7):816-880. DOI: 10.1016/j.pmatsci.2005.04.001
3. Stanley JK, Yensen TD. Hiperco - A Magnetic Alloy. AIEE Transactions. 1947;66:714-718.
4. CD Pitt, RD.Rawlings. Lüders strain and ductility of ordered Fe–Co–2V and Fe–Co–V–Ni alloys, Metal Science. 1983;17(6):261-266. DOI: 10.1179/030634583790420835
5. Duckham A, Zhang D, Liang D. Luzin V, Cammarata, R., Leheny, R., Weihs, T. (2003). Temperature dependent mechanical properties of ultra-fine grained FeCo–2V. Acta Materialia, 51(14), 4083-4093. doi:10.1016/s1359-6454(03)00228-3
6. Kustas AB, Susan DF, Johnson KL, Whetten SR, Rodriguez MA, Dagel DJ, Argibay N. Characterization of the Fe-Co-1.5V soft ferromagnetic alloy processed by Laser Engineered Net Shaping (LENS). Additive Manufacturing. 2018;21:41-52. DOI: 10.1016/j.addma.2018.02.006
7. Ren L, Hai Yu, R, Xiao JQ, Parvizi-Majidi A. Mechanical Properties of Fe-Co Soft Magnets. Journal of Materials Science. 2001;36:1451-1457.
8. Nabi B, Helbert A, Brisset F, André G, Waeckerlé T, Baudin T. Effect of recrystallization and degree of order on the magnetic and mechanical properties of soft magnetic FeCo–2V alloy. Materials Science and Engineering: A. 20163;578:215-221. DOI: 10.1016/j.msea.2013.04.066
9. Susan D, Crenshaw T, Rodelas J, Robino C, Greenwood B. Unpublished work; 2014.
10. Budynas RG, Nisbett JK. Materials. Fatigue Failure Resulting from Variable Loading in *Shigley's Mechanical Engineering Design* (10th ed.). New York, NY: McGraw-Hill Education. 2015;42-64.
11. Stoloff NS, Choe SJ, Rajan K. The Influence of Long Range Order on Fatigue Crack Initiation in an FeCo-V Intermetallic Compound. Scripta Metallurgica Et Materialia. 1992;26:331-336.

12. ASTM International. ASTM E606/E606M-12 Standard Test Method for Strain-Controlled Fatigue Testing; 2012. Available:https://doi-org.libproxy.unm.edu/10.1520/E0606_E0606M-12
13. Johnson AS, Shao S, Shamsaei N, Thompson SM, Bian L. Microstructure, Fatigue Behavior, and Failure Mechanisms of Direct Laser-Deposited Inconel 718. Jom. 2016;69(3):600-601. DOI: 10.1007/s11837-016-2225-2
14. Chapra SC, Canale RP. Least-Squares Regression. In Numerical Methods for Engineers with Software and Programming Applications (4th ed.). New York, NY: Mc Graw Hill. 2002;440-456
15. Khraishi TA, Al-Haik MS. Hardness Measurements. In *Experiments in Materials Science and Engineering* (1st ed.,). San Diego, CA: Cognella. 2011;43-64.
16. Kalpakjian S, Schmid SR. Failure and Fracture of Materials. In Manufacturing Engineering and Technology (7th ed., pp. 75-79). Singapore: Pearson Education Soout Asia Pte; 2014.
17. Kobayashi Y, Suzuki H. Cobalt Occurrence, Uses and Properties (pp. 216-218). New York, NY: Nova Science Publishers, Inc.; 2013.
18. ntrs.nasa.gov/archive/nasa/casi.ntrs.nasa.gov/19650026369
19. Lewis G, Janna S. Effect of test specimen cross-sectional shape on the in vitro fatigue life of acrylic bone cement. Biomaterials. 2003;24(23):4315-4321.
20. Callister WD, Jr., Rethwisch DG. Chapter 7: Mechanical Properties. In Fundamentals of Materials Science and Engineering an Integrated Approach (4th ed.). Hoboken, NJ: John Wiley & Sons; 2012;200-259.
21. Available:https://www.askzn.co.za/stainless-steel/tech-grades.htm

Peer-review history:
The peer review history for this paper can be accessed here:
http://www.sdiarticle4.com/review-history/61050